Journal of Biomedical Optics

BiomedicalOptics.SPIEDigitalLibrary.org

Optical oximetry of volume-oscillating vascular compartments: contributions from oscillatory blood flow

Jana M. Kainerstorfer
Angelo Sassaroli
Sergio Fantini

SPIE.

Optical oximetry of volume-oscillating vascular compartments: contributions from oscillatory blood flow

Jana M. Kainerstorfer,*,† Angelo Sassaroli, and Sergio Fantini
Tufts University, Department of Biomedical Engineering, 4 Colby Street, Medford, Massachusetts 02155, United States

Abstract. We present a quantitative analysis of dynamic diffuse optical measurements to obtain oxygen saturation of hemoglobin in volume oscillating compartments. We used a phasor representation of oscillatory hemodynamics at the heart rate and respiration frequency to separate the oscillations of tissue concentrations of oxyhemoglobin (**O**) and deoxyhemoglobin (**D**) into components due to blood volume (subscript V) and blood flow (subscript F): $\mathbf{O} = \mathbf{O}_V + \mathbf{O}_F$, $\mathbf{D} = \mathbf{D}_V + \mathbf{D}_F$. This is achieved by setting the phase angle $\mathrm{Arg}(\mathbf{O}_F) - \mathrm{Arg}(\mathbf{O})$, which can be estimated by a hemodynamic model that we recently developed. We found this angle to be −72 deg for the cardiac pulsation at 1 Hz, and −7 deg for paced breathing at 0.1 Hz. Setting this angle, we can obtain the oxygen saturation of hemoglobin of the volume-oscillating vascular compartment, $S_V = |\mathbf{O}_V|/(|\mathbf{O}_V| + |\mathbf{D}_V|)$. We demonstrate this approach with cerebral near-infrared spectroscopy measurements on healthy volunteers at rest ($n = 4$) and during 0.1 Hz paced breathing ($n = 3$) with a 24-channel system. Rest data at the cardiac frequency were used to calculate the arterial saturation, $S^{(a)}$; over all subjects and channels, we found $\langle S_V \rangle = \langle S^{(a)} \rangle = 0.96 \pm 0.02$. In the case of paced breathing, we found $\langle S_V \rangle = 0.66 \pm 0.14$, which reflects venous-dominated hemodynamics at the respiratory frequency. [DOI: 10.1117/1.JBO.21.10.101408]

Keywords: near-infrared spectroscopy; pulse oximetry; oxygen saturation of hemoglobin; vascular compartment; arterial saturation; venous saturation.

Paper 150691SSR received Oct. 14, 2015; accepted for publication Jan. 26, 2016; published online Mar. 1, 2016.

1 Introduction

1.1 *Arterial Saturation Measurements by Pulse Oximetry: From the Finger to the Brain*

Pulse oximetry is a technique that is based on the optical measurement of blood volume changes (photoplethysmography) to measure the arterial saturation, $S^{(a)}$, in tissue noninvasively. It is the most used optical technique in clinical routines since the mid-1980s.[1,2] The basis of pulse oximetry is to measure the optical spectral signature of the arterial pulsatile signal at the cardiac frequency. Typically, two wavelengths of light, one in the red and one in the near-infrared region, are used for illuminating an extremity, such as the fingertip, and measuring the transmitted light intensity. Every time the heart is pumping blood, arteries are expanding in diameter, hence arterial blood volume increases. Such an increase in blood volume results in a greater hemoglobin concentration in tissue and a higher absorption, hence a reduction in the detected light from the tissue. Since oxyhemoglobin and deoxyhemoglobin have distinguishably different wavelength-dependent absorption coefficients, the ratio of the pulsatile components of the measured intensities at the two wavelengths can be translated into oxygen saturation of hemoglobin in the arteries, i.e., the arterial saturation. The pulsatile component is a measure of the amplitude of intensity oscillations at the heartbeat frequency.

Calculating $S^{(a)}$ from pulsatile intensities at two wavelengths can be achieved by applying the modified Beer–Lambert law,[3] which yields the pulsatile components of oxy- and deoxyhemoglobin concentrations, $\Delta O(t)$ and $\Delta D(t)$, respectively. However, the ratio of the differential path length factors (DPFs) at the two wavelengths needs to be known.[3] In the absence of this information, commercial pulse oximeters are based on an empirical calibration.[3,4] This is typically applied to healthy volunteers by calibrating optical measurements with actual $S^{(a)}$ values obtained on drawn arterial blood, in protocols that involve altering $S^{(a)}$ over a safe range by modulating the fraction of inspired oxygen (FiO_2). A key assumption in order to calculate the arterial saturation through the procedure described above is that the pulsatile intensity component originates only from the arterial blood volume. The error associated with finger pulse oximetry systems is typically reported by manufacturers to be 2%, evaluated by the standard deviation of the differences between pulse oximetry signals and actual concurrent measurements of $S^{(a)}$ by drawing blood in healthy subjects.[4] However, a standard deviation of 2% reflects an expected error of 4% (two standard deviations) or more in 5% of the examinations, which also corresponds to an error of 3% to 4% reported in clinical studies and even greater for $S^{(a)} < 80\%$.[5,6]

Reflectance-based pulse oximeters have also been proposed.[7,8] Using a reflectance geometry on the subject's forehead has a considerable advantage over finger or toe sensors, since

*Address all correspondence to: Jana M. Kainerstorfer, E-mail: jkainers@andrew.cmu.edu

†Present address: Carnegie Mellon University, Department of Biomedical Engineering, 700 Technology Drive, Pittsburgh, Pennsylvania 15219, United States.

the extremities may be poorly perfused, which reduces the pulsatile signal to be measured. However, the pulsatile waveform measured on the forehead with a source–detector distance of about 1 cm has been found to be less reliable, or rather poorly understood, and readings of $S^{(a)}$ tend to be underestimated.[3,9] One possible proposed explanation is that the sensor actually picks up a contribution from a venous pulsation, so that the resulting readings reflect a mixture of arterial and venous saturation.[9,10] However, the reasoning for contributing venous readings as source of error was only based on the fact that the readings on the forehead have been underestimating $S^{(a)}$. It has further been found that the readings on the forehead improved when applying a mild pressure to the forehead sensor.[9,10] It shall be pointed out though that venous pulsation has not been measured directly. Furthermore, contributions of venous pulsatile volume change to the measured optical signals can be considered negligible in comparison to arterial volume changes due to the fact that pulsatile arterial pressure is significantly greater than any pulsatile component in the central venous pressure. It is more likely, as argued in this article, that inaccurate readings of arterial saturation from pulsatile optical signals are due to pulsatile blood flow contributions, rather than pulsatile venous contributions.

While forehead sensors with small source–detector separations seem to eliminate possible errors by applying pressure on the sensor, cerebral measurements with large source detector distances (~3 cm) cannot benefit from such maneuver. Measuring the cerebral concentration and oxygen saturation of hemoglobin at relatively large source–detector distances and two optical wavelengths is accomplished by the noninvasive technique of near-infrared spectroscopy (NIRS), which typically is used to report changes in oxy- and deoxyhemoglobin as a function of time.

While the contribution from a pulsatile venous blood volume change is questionable, it is known that capillary blood flow has a pulsatile component[11,12] that may also affect the measured signals. The oxygen saturation of hemoglobin in blood changes as the blood flows through the smaller arterioles and capillary bed due to oxygen diffusion to the surrounding tissue. Consequently, a pulsatile capillary blood flow may influence the reading of $S^{(a)}$ by pulse oximetry, due to the flow-related change in the tissue concentrations of oxy- and deoxyhemoglobin. A contribution of blood flow changes to the measured optical signals would result in oscillations of oxy- and deoxyhemoglobin, which are out of phase with each other[13] and hence would influence the reading of $S^{(a)}$. We have repeatedly shown that oxy- and deoxyhemoglobin measurements on muscle tissue are in phase[14] at the respiratory frequency, indicating that blood volume changes are dominant and blood flow changes can be considered negligible. However, cerebral measurements have shown a consistent out of phase behavior between oxy- and deoxyhemoglobin,[14–19] indicating that blood flow changes are not a negligible contributor to the optical signals. The reason for this is that blood volume changes are smaller in the brain than other tissues due to the rigid enclosure of the skull,[20] damping the magnitude of vessel diameter changes. Since the amplitude of the pulsatile blood volume changes is smaller, it is to be expected that the influence of pulsatile blood flow on $S^{(a)}$ measurements by pulse oximetry may be greater in the brain than other tissue locations, such as the finger, toe, or earlobe. As stated above, the underlying assumption to use pulsatile intensity changes for arterial saturation measurements is that the pulsatile intensity originates only from arterial blood volume.[21] Any additional source of pulsatile intensity, be it from venous blood or pulsatile flow, invalidates the theory and negatively impacts the accuracy of arterial saturation measurements.

1.2 *Venous Saturation Measurements by Spiroximetry or Venous-Pooling-Based Methods*

Using the same idea that forms the basis of pulse oximetry, i.e., to measure the oxygen saturation of hemoglobin of a specific vascular compartment by exploiting blood volume changes specific to that compartment, NIRS methods for measurements of venous saturation, $S^{(v)}$, have also been proposed. Microvascular $S^{(v)}$ measurements are especially important for cerebral monitoring, since they provide indications about oxygen extraction (the oxygen extraction fraction) and cerebral metabolic demand. Instead of using pulsations at the cardiac frequency, which predominantly impact the arterial blood volume, it has been proposed that respiration-induced changes in the blood pressure and intrathoracic pressure mostly affect the venous compartment due to the much larger vascular compliance in veins with respect to arteries. Therefore, it was proposed that oscillating hemoglobin concentration changes at the respiratory frequency may be used to measure the venous saturation.[22–26] This method, sometimes called spiroximetry, has been applied in animal models and in human skeletal muscle,[22] and also to cerebral measurements in healthy subjects[24,25] and ventilated patients.[23,24,26] Spiroximetry is based on taking the ratio of amplitudes of oscillating signals (the envelope). Similar to pulse oximetry, spiroximetry is therefore only valid if volume changes are the sole source of signal changes. This implies that oxy- and deoxyhemoglobin are in phase with each other. It further implies and will be demonstrated here that blood flow changes at the respiration frequency will invalidate the assumptions made by spiroximetry. Measurements of oscillatory hemodynamics at the respiration rate are practically appealing for obtaining $S^{(v)}$ since they rely on spontaneous respiration and do not require any external maneuvers.

In addition to using oscillatory, respiration-induced hemodynamic changes, several other methods for eliciting venous volume changes have been proposed. For example, one method for cerebral measurements is based on a head-down tilting protocol; tilting the head down by 15 deg results in venous pooling and hence a venous volume change.[27] In this approach, the venous saturation is calculated from the difference in the cerebral concentrations of oxy- and deoxyhemoglobin before and after head tilting. Another example, for measurements on fingers, involves eliciting venous volume changes by venous occlusion.[4,28] Again, the difference in hemoglobin concentration before occlusion and during occlusion is used for the measurement of $S^{(v)}$. While these latter measurements have shown promise in body parts where venous occlusions are possible, applications to cerebral venous saturation are limited. For brain measurements, the head-tilting method has its own limitations, which includes some reliability issues in the induced hemodynamic changes,[27] a possible arterial contribution, and potential optical path length changes due to head tilting.

Similar to the case of pulse oximetry, these methods for venous saturation measurement also rely on the same assumption that a specific vascular compartment (venous in this case) dominates the blood volume changes that contribute to the optical signals.

1.3 *Accounting for Contributions from Blood Flow Oscillations*

While venous blood volume oscillations are indeed a major contributor to the optical signals at the respiration frequency, we have recently demonstrated that blood flow oscillations may also play a crucial role and need to be accounted for.[13,16,29] This result follows from a hemodynamic model that we have recently introduced, which translates oscillatory changes in cerebral blood volume (CBV) and cerebral blood flow (CBF) into changes in the tissue concentrations of oxyhemoglobin, ΔO, and deoxyhemoglobin, ΔD. This model, combined with inducing hemodynamic oscillations at a set of controlled frequencies, has led to the new technique of coherent hemodynamics spectroscopy,[13,14,16,18] which aims at a quantitative assessment of the microcirculation.

In our previous applications of the hemodynamic model, which is an analytical model that takes into account dynamic autoregulation and the microvascular blood transit times, we have focused on low-frequency cerebral hemodynamics (of the order of 0.1 Hz or less)[13–18,29] for the assessment of blood flow, autoregulation, and blood volume in the microvasculature. In this work, we demonstrate that the pulsatile signals measured in the brain at the heart rate and at the respiration frequency can be quantitatively described by the model and that CBF changes should be taken into account to obtain reliable measurements of the oxygen saturation of hemoglobin of time-varying vascular compartments. We propose a method, based on our hemodynamic model, which allows for the separation of the contributions of pulsatile blood volume and blood flow to the measured oscillations of hemoglobin concentration. This method yields measurements of the oxygen saturation of hemoglobin of the volume-oscillating vascular compartment, be it arterial, venous, or a combination of both, that take into account the potentially confounding contributions from oscillatory blood flow.

2 Methods

2.1 *Analytical Hemodynamic Model*

We have recently introduced a hemodynamic model, which describes time-dependent expressions of the absolute tissue concentrations of $O(t)$, $D(t)$, and $T(t)$ (with units of micromoles per liter of tissue) as a function of dynamic changes of CBV and CBF normalized to baseline ($\mathrm{cbv}(t) = \Delta\mathrm{CBV}(t)/\mathrm{CBV}_0$, $\mathrm{cbf}(t) = \Delta\mathrm{CBF}(t)/\mathrm{CBF}_0$). Dynamic changes in the metabolic rate of oxygen, cmro_2, are also considered by the model but they are neglected here because we are considering cases where cerebral hemodynamics is dominated by blood volume and blood flow changes. In general, the time evolution of hemoglobin concentrations in tissue depends on both cbv and cbf (again, we neglect cmro_2 here). The measurable, dynamic and hence time-dependent quantities of $O(t)$ and $D(t)$ can be written as the sum of dynamic blood flow and blood volume contributions, indicated with subscripts F and V, respectively:

$$O(t) = O_F(t) + O_V(t), \tag{1}$$

$$D(t) = D_F(t) + D_V(t). \tag{2}$$

The subscripts "V" and "F" refer to dynamic changes in $O(t)$ and $D(t)$ resulting from dynamic changes in volume and flow, hence due to $\mathrm{cbv}(t)$ and $\mathrm{cbf}(t)$. The hemodynamic model describes explicitly how given $\mathrm{cbf}(t)$ and $\mathrm{cbv}(t)$ yield $O_F(t)$, $O_V(t)$, $D_F(t)$, and $D_V(t)$. Specifically, the model derives temporal dynamics (time-domain description) of hemoglobin changes, as well as sinusoidal hemodynamic oscillations as a function of the angular frequency ω (frequency-domain description). Here, we adopt the frequency-domain version of the model for describing oscillating hemodynamic signals such as those related to cardiac pulsation and respiration. We adopted the phasor representation of oscillatory quantities, where phasors are indicated in boldface. By definition, phasors (boldface) are dynamic quantities. The model expressions for $\mathbf{O}(\omega)$, $\mathbf{D}(\omega)$, $\mathbf{T}(\omega)$ (i.e., the phasors that describe the oscillations of the oxy-, deoxy-, and total hemoglobin concentrations, respectively) as a function of $\mathbf{cbv}(\omega)$ and $\mathbf{cbf}(\omega)$ (i.e., the phasors that describe the oscillations of CBV and CBF) are as follows:[13,16]

$$\mathbf{O}(\omega) = \mathbf{O}_V(\omega) + \mathbf{O}_F(\omega), \tag{3}$$

$$\mathbf{O}_V(\omega) = \mathrm{ctHb}[S^{(a)}\mathrm{CBV}_0^{(a)}\mathbf{cbv}^{(a)}(\omega) + S^{(v)}\mathrm{CBV}_0^{(v)}\mathbf{cbv}^{(v)}(\omega)], \tag{4}$$

$$\mathbf{O}_F(\omega) = \mathrm{ctHb}\left[\frac{\langle S^{(c)}\rangle}{S^{(v)}}(\langle S^{(c)}\rangle - S^{(v)})\mathcal{F}^{(c)}\mathrm{CBV}_0^{(c)}\mathcal{H}_{LP}^{(c)}(\omega) + (S^{(a)} - S^{(v)})\mathrm{CBV}_0^{(v)}\mathcal{H}_{LP}^{(v)}(\omega)\right][\mathbf{cbf}(\omega)], \tag{5}$$

$$\mathbf{D}(\omega) = \mathbf{D}_V(\omega) + \mathbf{D}_F(\omega), \tag{6}$$

$$\mathbf{D}_V(\omega) = \mathrm{ctHb}[(1 - S^{(a)})\mathrm{CBV}_0^{(a)}\mathbf{cbv}^{(a)}(\omega) + (1 - S^{(v)})\mathrm{CBV}_0^{(v)}\mathbf{cbv}^{(v)}(\omega)], \tag{7}$$

$$\mathbf{D}_F(\omega) = -\mathrm{ctHb}\left[\frac{\langle S^{(c)}\rangle}{S^{(v)}}(\langle S^{(c)}\rangle - S^{(v)})\mathcal{F}^{(c)}\mathrm{CBV}_0^{(c)}\mathcal{H}_{LP}^{(c)}(\omega) + (S^{(a)} - S^{(v)})\mathrm{CBV}_0^{(v)}\mathcal{H}_{LP}^{(v)}(\omega)\right][\mathbf{cbf}(\omega)], \tag{8}$$

$$\mathbf{T}(\omega) = \mathrm{ctHb}[\mathrm{CBV}_0^{(a)}\mathbf{cbv}^{(a)}(\omega) + \mathrm{CBV}_0^{(v)}\mathbf{cbv}^{(v)}(\omega)], \tag{9}$$

where $\mathcal{H}_{LP}^{(c)}(\omega)$ and $\mathcal{H}_{LP}^{(v)}(\omega)$ are the complex transfer functions associated with blood circulation in the capillary bed [$\mathcal{H}_{LP}^{(c)}(\omega)$, approximated by a resistor-capacitor (RC) low-pass filter, which contains as a parameter the capillary transit time $t^{(c)}$] and in the venous compartment [$\mathcal{H}_{LP}^{(v)}(\omega)$, approximated by a time-shifted Gaussian low-pass filter, which contains as parameters the capillary transit time $t^{(c)}$ and the venous transit time $t^{(v)}$], ctHb is the hemoglobin concentration in blood, $\mathcal{F}^{(c)}$ is the Fåhraeus factor (ratio of capillary-to-large vessel hematocrit), and the superscripts (a), (c), and (v) for CBV, cbv, and oxygen saturation of hemoglobin S indicate their values associated with the arterial, capillary, and venous compartments, respectively. The total, steady state blood volume is given by $\mathrm{CBV}_0 = \mathrm{CBV}_0^{(a)} + \mathcal{F}^{(c)}\mathrm{CBV}_0^{(c)} + \mathrm{CBV}_0^{(v)}$, where $\mathrm{CBV}_0^{(a)}$, $\mathrm{CBV}_0^{(c)}$, and $\mathrm{CBV}_0^{(v)}$ correspond to the baseline contributions of blood volume in the arterial, capillary, and venous compartment, respectively. Boldface lowercase, quantities correspond to dynamic changes

relative to baseline values. We have set $\mathbf{cbv}^{(c)}(\omega) = 0$ since dynamic dilation and recruitment of capillaries in brain tissue are negligible.[30–35] Note that the only measurable parameters in Eqs. (1)–(9) are $|\mathbf{O}(\omega)|$, $|\mathbf{D}(\omega)|$, $|\mathbf{T}(\omega)|$, $\mathrm{Arg}(\mathbf{D}) - \mathrm{Arg}(\mathbf{O})$, and $\mathrm{Arg}(\mathbf{O}) - \mathrm{Arg}(\mathbf{T})$. Finally, we observe that one can define an overall blood volume phasor, $\mathbf{cbv}(\omega)$, as follows:

$$\mathbf{cbv}(\omega) = \frac{\mathrm{CBV}_0^{(a)}}{\mathrm{CBV}_0}\mathbf{cbv}^{(a)}(\omega) + \frac{\mathrm{CBV}_0^{(v)}}{\mathrm{CBV}_0}\mathbf{cbv}^{(v)}(\omega), \tag{10}$$

so that, as seen in Eq. (9), the phasor of total hemoglobin concentration, $\mathbf{T}(\omega)$, has the same phase as $\mathbf{cbv}(\omega)$.

2.2 *Derivation of the Basic System of Phasor Equations That Describes Cerebral Hemodynamics*

We now make the key assumption that arterial and venous blood volumes oscillate in phase, which should be the case when blood volume oscillations are driven by systemic blood pressure changes. In other words, the phasors, $\mathbf{cbv}^{(a)}(\omega)$, $\mathbf{cbv}^{(v)}(\omega)$, and $\mathbf{cbv}(\omega)$, have the same phase. Under these conditions, Eq. (10) directly translates into a condition for the magnitudes of the blood volume phasors:

$$|\mathbf{cbv}(\omega)| = \frac{\mathrm{CBV}_0^{(a)}}{\mathrm{CBV}_0}|\mathbf{cbv}^{(a)}(\omega)| + \frac{\mathrm{CBV}_0^{(v)}}{\mathrm{CBV}_0}|\mathbf{cbv}^{(v)}(\omega)|. \tag{11}$$

One may introduce a factor, $\rho^{(v)}$ with $0 \le \rho^{(v)} \le 1$, that specifies the venous fraction of the total oscillating blood volume as follows:

$$\rho^{(v)} = \frac{\mathrm{CBV}_0^{(v)}|\mathbf{cbv}^{(v)}|}{\mathrm{CBV}_0|\mathbf{cbv}|}, \tag{12}$$

from which the arterial fraction of the total oscillating blood volume is

$$\rho^{(a)} = 1 - \rho^{(v)} = \frac{\mathrm{CBV}_0^{(a)}|\mathbf{cbv}^{(a)}|}{\mathrm{CBV}_0|\mathbf{cbv}|}. \tag{13}$$

We point out that $\rho^{(v)}$ and $\rho^{(a)}$ depend on the nature of the oscillatory hemodynamics, and, in general, they also depend on ω. The condition of Eq. (11) and the definition of $\rho^{(v)}$ in Eq. (12) allow us to express the blood volume components of the oxy- and deoxyhemoglobin phasors of Eqs. (4) and (7) as follows:

$$\mathbf{O}_V(\omega) = \mathrm{ctHb}\,\mathrm{CBV}_0[(1-\rho^{(v)})S^{(a)} + \rho^{(v)}S^{(v)}]\mathbf{cbv}(\omega), \tag{14}$$

$$\mathbf{D}_V(\omega) = \mathrm{ctHb}\,\mathrm{CBV}_0[1-(1-\rho^{(v)})S^{(a)} - \rho^{(v)}S^{(v)}]\mathbf{cbv}(\omega). \tag{15}$$

Finally, by introducing the oxygen saturation of hemoglobin of the volume oscillating compartment $S_V = |\mathbf{O}_V|/|\mathbf{T}|$, one finds that it can be written as a weighted average of the arterial saturation ($S^{(a)} = |\mathbf{O}_V^{(a)}|/|\mathbf{T}^{(a)}|$) and venous saturation ($S^{(v)} = |\mathbf{O}_V^{(v)}|/|\mathbf{T}^{(v)}|$), with the weights given by the respective arterial and venous fractions of oscillating blood volume:

$$\begin{aligned} S_V &= \frac{|\mathbf{O}_V|}{|\mathbf{T}|} = \frac{|\mathbf{O}_V^{(a)}| + |\mathbf{O}_V^{(v)}|}{|\mathbf{T}^{(a)}| + |\mathbf{T}^{(v)}|} = (1-\rho^{(v)})\frac{|\mathbf{O}_V^{(a)}|}{|\mathbf{T}^{(a)}|} + \rho^{(v)}\frac{\mathbf{O}_V^{(v)}|}{\mathbf{T}^{(v)}|} \\ &= (1-\rho^{(v)})S^{(a)} + \rho^{(v)}S^{(v)}. \end{aligned} \tag{16}$$

With these definitions, the model equations for $\mathbf{O}_V$ and $\mathbf{D}_V$ become

$$\mathbf{O}_V(\omega) = \mathrm{ctHb}\,\mathrm{CBV}_0 S_V \mathbf{cbv}(\omega), \tag{17}$$

$$\mathbf{D}_V(\omega) = \mathrm{ctHb}\,\mathrm{CBV}_0(1-S_V)\mathbf{cbv}(\omega). \tag{18}$$

We are now in a position to write the system of phasor equations that describes cerebral hemodynamics driven by blood volume and blood flow oscillations:

$$\begin{cases} \mathbf{O}(\omega) = \mathbf{O}_V(\omega) + \mathbf{O}_F(\omega) \\ \mathbf{D}(\omega) = \mathbf{D}_V(\omega) + \mathbf{D}_F(\omega) \\ S_V\mathbf{D}_V(\omega) = (1-S_V)\mathbf{O}_V(\omega) \\ \mathbf{D}_F(\omega) = -\mathbf{O}_F(\omega) \end{cases}, \tag{19}$$

with the condition $0 \le S_V \le 1$. The first two equations in Eq. (19) repeat Eqs. (3) and (6), the third equation follows directly from Eqs. (17) and (18), and the fourth equation follows directly from Eqs. (5) and (8). By recalling that phasors are two-dimensional vectors, Eq. (19) is a linear system of eight scalar equations in nine unknowns (the components of the phasors $\mathbf{O}_V$, $\mathbf{O}_F$, $\mathbf{D}_V$, $\mathbf{D}_F$ and S_V), so that one needs to add one more condition to fully solve it. Two relevant scenarios are presented in the next two sections.

2.3 *Setting the Oxygen Saturation of Hemoglobin of the Volume-Oscillating Vascular Compartment*

One approach to fully solve the system of Eq. (19) is to set the value of S_V, the oxygen saturation of hemoglobin of the volume oscillating vascular compartment. Figure 1 shows a representative phasor diagram for the general case in which blood flow oscillations significantly contribute to the hemoglobin concentration oscillations. Here, we take the phase of $\mathbf{O}$ as the phase reference [so that $\mathrm{Arg}(\mathbf{O})$ is zero by definition]. Based on phasor algebra or a geometrical analysis of Fig. 1, one can derive the following solution to the linear system of Eq. (19):

$$O_{Vx} = S_V(O_x + D_x), \tag{20}$$

$$O_{Vy} = S_V D_y, \tag{21}$$

$$O_{Fx} = (1-S_V)O_x - S_V D_x, \tag{22}$$

$$O_{Fy} = -S_V D_y, \tag{23}$$

$$D_{Vx} = (1-S_V)(O_x + D_x), \tag{24}$$

$$D_{Vy} = (1-S_V)(D_y), \tag{25}$$

$$D_{Fx} = -[(1-S_V)O_x - S_V D_x], \tag{26}$$

$$D_{Fy} = S_V D_y, \tag{27}$$

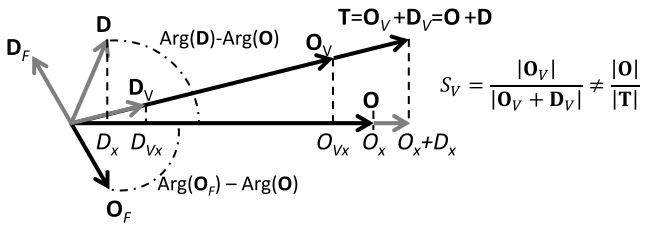

Fig. 1 Phasor diagram for **O**, **D**, and **T**, with blood flow contributions being non-negligible. It is easy to see that in this case, $[|\mathbf{O}|/(|\mathbf{O}|+|\mathbf{D}|)] < [|\mathbf{O}|/(|\mathbf{O}+\mathbf{D}|)]$ and neither expression yields S_V, which is given by $|\mathbf{O}_V|/(|\mathbf{O}_V+\mathbf{D}_V|)$.

where the subscripts x and y indicate the x and y components, respectively, of the corresponding phasor. Note that by taking the phase of **O** as the phase reference, **O** only has an x component ($O_y = 0$).

By inspecting Fig. 1, one may appreciate that the phasor representation leads to an easy, graphical solution of the system of Eq. (19). In fact, one may start by drawing the phasors **O**, **D**, and **T**, which are the measured phasors in an experiment. Then, based on the assumed value of the oxygen saturation of hemoglobin of the time-varying vascular compartment (S_V), one can draw $\mathbf{O}_V$ and $\mathbf{D}_V$ along the direction of **T**, as given by $\mathbf{O}_V = S_V\mathbf{T}$ and $\mathbf{D}_V = (1-S_V)\mathbf{T}$. Then, considering that $\mathbf{O} = \mathbf{O}_V + \mathbf{O}_F$ and $\mathbf{D} = \mathbf{D}_V + \mathbf{D}_F$, $\mathbf{O}_F$ and $\mathbf{D}_F$ can be drawn as the phasors from the tip of $\mathbf{O}_V$ to the tip of **O** and from the tip of $\mathbf{D}_V$ to the tip of **D**, respectively.

2.4 *Setting the Angle Between* **O** *and* $\mathbf{O}_F$

An alternative approach to setting S_V, the case described in the previous section, is to set the angle between the **O** and $\mathbf{O}_F$ phasors. To appreciate the meaning of this assumption, one needs to consider the blood flow phasor (**cbf**) and its phase relationship with the corresponding oxyhemoglobin concentration phasor ($\mathbf{O}_F$).

Let us first consider the phasor **cbf**. As mentioned above, Eqs. (9) and (10) show that the measured total hemoglobin phasor **T** is in phase with the blood volume phasor **cbv**. Because of the high-pass nature of the cerebral autoregulation process that regulates CBF in response to blood pressure changes,[36–38] we consider the following high-pass relationship between **cbf** and **cbv**:[13]

$$\mathbf{cbf}(\omega) = k\mathcal{H}_{\mathrm{HP}}^{(\mathrm{AR})}(\omega)\mathbf{cbv}(\omega), \tag{28}$$

where k is the inverse of the modified Grubb's exponent, and $\mathcal{H}_{HP}^{(\mathrm{AR})}(\omega)$ is the RC high-pass transfer function with cutoff frequency $f_c^{(\mathrm{AR})}$ that describes the effect of autoregulation ($f_c^{(\mathrm{AR})} \sim 0.03 - 0.05$ Hz). Equation (28) quantitatively describes the relationship between the **cbf** and **cbv** phasors in terms of a simple high-pass transfer function. While the specific quantitative aspects of this relationship may be improved by more sophisticated models of autoregulation (possibly considering also the relationship between blood volume and blood pressure, the latter being the quantity directly involved with autoregulation), the qualitative relationship between **cbf** and **cbv** is correctly described by Eq. (28). Specifically, at higher frequencies (say, at the heartbeat frequency), **cbf** and **cbv** are in phase, whereas at lower frequencies (say, at the frequency of normal breathing), **cbf** leads **cbv**. The specific angle by which **cbf** leads **cbv** depends on the autoregulation model used, and here we adopt the model of Eq. (28) based on an RC high-pass transfer function with $f_c^{(\mathrm{AR})} = 0.03$ Hz.

Let us now consider the phasor $\mathbf{O}_F$, which describes the oxyhemoglobin concentration oscillations that are induced by blood flow oscillations. $\mathbf{O}_F$ is not in phase with **cbf** because the effects of a change in blood flow on the concentration of oxyhemoglobin are mediated by the blood transit time in the microcirculation. This effect is quantitatively described by Eq. (5) of the hemodynamic model, where the low-pass transfer functions associated with capillary ($\mathcal{H}_{LP}^{(c)}$) and venous ($\mathcal{H}_{LP}^{(v)}$) flow account for the fact that $\mathbf{O}_F$ lags **cbf**. The characteristic times of the capillary and venous transfer functions are on the order of $t^{(c)}/e = 0.37t^{(c)}$ and $0.28(t^{(c)}+t^{(v)})$, respectively.[13] In this work, we use Eqs. (5) and (28) to estimate the phase of $\mathbf{O}_F$ (and therefore, the angle between **O** and $\mathbf{O}_F$), but other methods may also be used on the basis of different hemodynamic and autoregulation models.

By setting the phase angle of $\mathbf{O}_F$ with respect to **O** (we refer to this angle as $[\mathrm{Arg}(\mathbf{O}_F) - \mathrm{Arg}(\mathbf{O})] = \mathrm{Arg}(\mathbf{O}_F)$), one can immediately find an expression for S_V. In fact, by definition, $(\mathrm{O}_{Fy}/\mathrm{O}_{Fx}) = \tan[\mathrm{Arg}(\mathbf{O}_F)]$, and after replacing O_{Fx} and O_{Fy} with their expressions given in Eqs. (22) and (23), one finds

$$S_V = \frac{O_x\tan[\mathrm{Arg}(\mathbf{O}_F)]}{(O_x+D_x)\tan[\mathrm{Arg}(\mathbf{O}_F)] - D_y}. \tag{29}$$

By replacing S_V in Eqs. (20)–(27) with the expression of Eq. (29), one finds the full solution to the system of Eq. (19). As in the case of the previous section, the phasor diagram of Fig. 1 can be used to yield a graphical solution of the system of Eq. (19). In fact, after assuming the angle between **O** and $\mathbf{O}_F$, i.e., the direction of the oxyhemoglobin phasor associated with blood flow oscillations, one finds the tips of $\mathbf{O}_V$ and $\mathbf{D}_V$ (and therefore, $S_V = |\mathbf{O}_V|/|\mathbf{T}|$) by intersecting the **T** phasor with the line parallel to $\mathbf{O}_F$ that passes through the tip of **O** and **D**, respectively.

If the dynamics of the tissue concentrations of oxy- and deoxyhemoglobin are dominated by blood volume changes, with negligible contributions from blood flow changes, **O** and **D** are in phase with each other and only have x components, so that $D_y = 0$. Therefore, Eq. (29) shows that in this case, the oxygen saturation of hemoglobin of the volume oscillating compartment, S_V, is simply given by the amplitude ratio of the oxyhemoglobin to total hemoglobin oscillations:

$$S_V = \frac{O_x}{O_x+D_x} = \frac{|\mathbf{O}|}{|\mathbf{T}|}. \tag{30}$$

2.5 *Measuring the Arterial Saturation from Volume Oscillations at the Heart Rate*

At the cardiac pulsation frequency [heart rate: $\omega_{\mathrm{hr}}/(2\pi) \approx 1$ Hz], venous volume changes are negligible (because the pulsatile venous pressure is much less than the pulsatile arterial pressure), hence, $\mathbf{cbv}^{(v)}(\omega_{\mathrm{hr}}) \approx 0$. Furthermore, if one can also assume that the blood volume contributions to $\mathbf{O}(\omega)$ and $\mathbf{D}(\omega)$ are much greater than the blood flow contributions [i.e., $|\mathbf{O}_V(\omega)| \gg |\mathbf{O}_F(\omega)|$, $|\mathbf{D}_V(\omega)| \gg |\mathbf{D}_F(\omega)|$], one can calculate the arterial saturation, $S^{(a)}$, from the magnitudes of the phasors $\mathbf{O}(\omega_{\mathrm{hr}})$ and $\mathbf{D}(\omega_{\mathrm{hr}})$, as follows (case of negligible blood flow contributions):

$$\mathbf{O}_V^{(a)}(\omega_{\mathrm{hr}}) \approx \mathbf{O}_{\mathrm{V}}(\omega_{\mathrm{hr}}) \approx \mathrm{ctHb}[S^{(a)}\mathrm{CBV}_0^{(a)}\mathbf{cbv}^{(a)}(\omega_{\mathrm{hr}})], \quad (31)$$

$$\mathbf{D}_V^{(a)}(\omega_{\mathrm{hr}}) \approx \mathbf{D}_{\mathrm{V}}(\omega_{\mathrm{hr}}) \approx \mathrm{ctHb}[(1-S^{(a)})\mathrm{CBV}_0^{(a)}\mathbf{cbv}^{(a)}(\omega_{\mathrm{hr}})], \quad (32)$$

$$S^{(a)} = \frac{|\mathbf{O}_V^{(a)}(\omega_{\mathrm{hr}})|}{|\mathbf{T}(\omega_{\mathrm{hr}})|} \approx \frac{|\mathbf{O}_V(\omega_{\mathrm{hr}})|}{|\mathbf{T}(\omega_{\mathrm{hr}})|} \approx \frac{|\mathbf{O}(\omega_{\mathrm{hr}})|}{|\mathbf{T}(\omega_{\mathrm{hr}})|} \approx \frac{|\mathbf{O}(\omega_{\mathrm{hr}})|}{|\mathbf{O}(\omega_{\mathrm{hr}})| + |\mathbf{D}(\omega_{\mathrm{hr}})|}. \quad (33)$$

One can see that Eq. (33) is in agreement with Eq. (30), where S_V becomes $S^{(a)}$ in this case where the volume-oscillating vascular compartment is the arterial one. If blood volume changes are the only source of signal contributions, oxy- and deoxyhemoglobin changes occur simultaneously, so that the phase difference $\mathrm{Arg}[\mathbf{D}] - \mathrm{Arg}[\mathbf{O}] = 0$. Figure 2 illustrates the phasor diagram for this scenario of negligible blood flow contributions and blood volume contributions from solely arterial blood.

If, instead, blood flow oscillations yield non-negligible contributions to the measured hemoglobin concentrations, Eqs. (31)–(33) are not valid and one must take $\mathbf{O}_F$ and $\mathbf{D}_F$, and hence, the **cbf** terms in the model equations [Eqs. (5) and (8)], into account. Since $\mathbf{cbf}(\omega)$ introduces a phase shift (which is frequency dependent) between **O** and **D**, the phase difference $\mathrm{Arg}[\mathbf{D}] - \mathrm{Arg}[\mathbf{O}]$ is no longer 0. From this fact, it follows that $|\mathbf{O}_V| \neq |\mathbf{O}|$, and therefore (case of non-negligible blood flow contributions),

$$\begin{aligned}\mathbf{O}(\omega_{\mathrm{hr}}) = {} & \mathrm{ctHb}[S^{(a)}\mathrm{CBV}_0^{(a)}\mathbf{cbv}^{(a)}(\omega_{\mathrm{hr}})] \\ & + \mathrm{ctHb}\left[\frac{\langle S^{(c)}\rangle}{S^{(v)}}(\langle S^{(c)}\rangle - S^{(v)})\mathcal{F}^{(c)}\mathrm{CBV}_0^{(c)}\mathcal{H}_{LP}^{(c)}(\omega_{\mathrm{hr}}) \right. \\ & \left. + (S^{(a)} - S^{(v)})\mathrm{CBV}_0^{(v)}\mathcal{H}_{LP}^{(v)}(\omega_{\mathrm{hr}})\right][\mathbf{cbf}(\omega_{\mathrm{hr}})], \quad (34)\end{aligned}$$

$$\begin{aligned}\mathbf{D}(\omega_{\mathrm{hr}}) = {} & \mathrm{ctHb}\left[(1-S^{(a)})\mathrm{CBV}_0^{(a)}\mathbf{cbv}^{(a)}(\omega_{\mathrm{hr}})\right] \\ & - \mathrm{ctHb}\left[\frac{\langle S^{(c)}\rangle}{S^{(v)}}(\langle S^{(c)}\rangle - S^{(v)})\mathcal{F}^{(c)}\mathrm{CBV}_0^{(c)}\mathcal{H}_{LP}^{(c)}(\omega_{\mathrm{hr}}) \right. \\ & \left. + (S^{(a)} - S^{(v)})\mathrm{CBV}_0^{(v)}\mathcal{H}_{LP}^{(v)}(\omega_{\mathrm{hr}})\right][\mathbf{cbf}(\omega_{\mathrm{hr}})]. \quad (35)\end{aligned}$$

Equations (34) and (35) combine Eqs. (3)–(5) and (6)–(8), respectively, and specify that the oscillations are at the cardiac frequency (ω_{hr}).

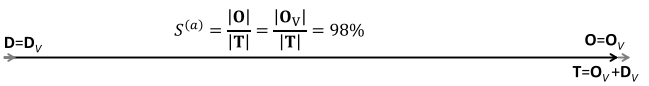

Fig. 2 Phasor diagram for the oxy- and deoxyhemoglobin phasors (**O** and **D**) at the cardiac pulsation frequency, with a negligible blood flow contribution. For this ideal case, **O** and **D** are in phase and the arterial saturation can be calculated as $|\mathbf{O}|/|\mathbf{O}+\mathbf{D}|$.

In this case of non-negligible blood flow contributions:

$$S^{(a)} = \frac{|\mathbf{O}_V^{(a)}(\omega_{\mathrm{hr}})|}{|\mathbf{T}(\omega_{\mathrm{hr}})|} \approx \frac{|\mathbf{O}_{\mathrm{V}}(\omega_{\mathrm{hr}})|}{|\mathbf{T}(\omega_{\mathrm{hr}})|} \neq \frac{|\mathbf{O}(\omega_{\mathrm{hr}})|}{|\mathbf{T}(\omega_{\mathrm{hr}})|}. \quad (36)$$

When **O** and **D** are not in phase with each other, it is important to point out that

$$\frac{|\mathbf{O}|}{|\mathbf{T}|} = \frac{|\mathbf{O}|}{|\mathbf{O}+\mathbf{D}|} \neq \frac{|\mathbf{O}|}{|\mathbf{O}|+|\mathbf{D}|}. \quad (37)$$

In summary, measuring the arterial saturation on the basis of the rightmost term in Eq. (33) is only correct if blood flow contributions to the measured oscillations of oxy- and deoxyhemoglobin are negligible.

2.6 *Measuring the Venous Saturation from Volume Oscillations at the Respiratory Frequency*

Similar to the way that heartbeat-induced hemodynamics have been used to measure arterial saturation, respiration-induced hemodynamic oscillations have been proposed to measure the venous saturation, $S^{(v)}$.[22–26] The idea is that at the respiration frequency, venous blood volume oscillations may be the dominant source of oxy- and deoxyhemoglobin concentration dynamics. Using these hemodynamic oscillations for calculating $S^{(v)}$ has led to a method of venous saturation measurements[16–19] for which the term spiroximetry was coined.[22] As shown above for the arterial saturation, if blood flow contributions are negligible, then $\mathrm{Arg}[\mathbf{D}] - \mathrm{Arg}[\mathbf{O}] = 0$. However, we have previously demonstrated,[13–16,29] and we will show again here that this is not the case for brain measurements, where blood flow contributions cannot be neglected. Hence, it is not correct to use the ratio $|\mathbf{O}|/|\mathbf{T}|$ to obtain $S^{(v)}$ from data collected during paced or normal breathing, since $\mathbf{O} \neq \mathbf{O}_V$.

While the value of arterial saturation $S^{(a)}$ can often be reliably assumed since it is a robust systemic parameter that takes values in a narrow range for healthy individuals (leading to the approach of Sec 2.3), the value of venous saturation depends on the specific, local conditions of oxygen supply (through blood flow) and oxygen delivery (to accommodate metabolic demand) of the tissue considered. Therefore, the measurement of oxygen saturation of hemoglobin in a volume-oscillating compartment that comprises venous blood can be achieved according to the approach of Sec. 2.4, where one assumes the phase of the flow component of the oxyhemoglobin concentration phasor ($\mathbf{O}_{\mathrm{F}}$) with respect to the total, measured phasor **O** (i.e., one assumes the value of $[\mathrm{Arg}(\mathbf{O}_F) - \mathrm{Arg}(\mathbf{O})]$).

In general, one should also consider the fact that arterial and venous blood may both contribute to the blood volume oscillations associated with the total hemoglobin concentration phasor: $\mathbf{T} = \mathbf{T}^{(a)} + \mathbf{T}^{(v)}$. The relative venous and arterial contributions to the oscillatory blood volume are quantified by the factors $\rho^{(v)}$ and $\rho^{(a)} = 1 - \rho^{(v)}$ introduced in Sec. 2.2. If $\rho^{(v)} = 1$, i.e., only venous blood contributes to **T**, then the oxygen saturation of hemoglobin of the volume-oscillating compartment (S_V) coincides with the venous saturation ($S^{(v)}$). Otherwise, in general, one needs to estimate $\rho^{(v)}$ to assess the contributions of arterial and venous saturation to S_V.

2.7 *Human Subjects*

Ten healthy subjects were recruited for the study (six males and four females, age range: 25 to 49 years) without any history of neurological disorders or cardiovascular disease. The experimental protocol was approved by the Tufts University Institutional Review Board (IRB). Written informed consent was obtained from all participants prior to the study. Subjects were seated in a darkened room and instructed to breathe normally. The experimental protocol consisted of acquiring 10 min of resting baseline measurements. In addition, three of the subjects performed 6.5 min of paced breathing at a frequency of 0.1 Hz, as guided by a metronome.

2.8 *Near-Infrared Spectroscopy Data Collection and Data Processing*

Optical data were collected with a commercial NIRS optical topography system (ETG 4000, Hitachi Medical Corporation, Japan), operating at wavelengths of 700 and 830 nm. Optical probes were placed on the subject's head, in the area corresponding to the frontal lobe, and secured by a dedicated cap to hold them in place. The probe consisted of eight illumination fibers and eight collection fibers, arranged in a grid, as seen in Fig. 3. The source–detector distance for all measurement channels was 3 cm; there was a total of 24 source–detector pairs (or measurement channels), with each channel acquiring data with a 10-Hz sampling frequency.

After removing slow temporal drifts from the NIRS data, optical intensity changes were translated into relative changes of $\Delta O(t)$, $\Delta D(t)$, and $\Delta T(t)$ (oxy-, deoxy, and total hemoglobin concentrations, respectively) by applying the modified Beer–Lambert law to each channel. A DPF ratio of $\mathrm{DPF}_{700}/\mathrm{DPF}_{830} = 1$ (specifically: $\mathrm{DPF}_{700} = \mathrm{DPF}_{830} = 6.51$) was used unless otherwise stated.

The fast Fourier transform (FFT) was taken for each channel's intensity time trace, normalized to its baseline value ($\Delta I(t)/I_0$, where $\Delta I(t) = I(t) - I_0$) for both wavelengths. The baseline value I_0 is defined as the mean value over the entire time trace. Only those channels for which the magnitude of the Fourier transform at the cardiac frequency (for the baseline measurements) or at 0.1 Hz (for the paced breathing measurements) was at least 5 times greater than the average magnitude of the Fourier transform at frequencies >4 Hz have been considered for further processing. The other channels were discarded because considered insensitive to cerebral hemodynamics and dominated by noise. In addition, only those subjects with at least 20 channels meeting this criterion were included for further processing. Four out of 10 subjects satisfied this requirement for baseline measurements, and 3 out of 3 subjects for paced breathing measurements.

In order to study the phase relationship, as well as the amplitudes, of the pulsatile signals, relative intensities at each wavelength, $\Delta I_{700}(t)/I_{0\_700}$ and $\Delta I_{830}(t)/I_{0\_830}$, as well as $\Delta O(t)$, $\Delta D(t)$, and $\Delta T(t)$, were band-pass filtered around the cardiac frequency, which was in the range 0.96 to 1.2 Hz in this study (filter width: ± 0.2 Hz; filter order: $n = 214$) for the baseline dataset, and around 0.1 Hz (filter width: ± 0.02 Hz; filter order: $n = 536$) for the paced breathing data with a linear-phase band-pass filter (function "firpmord" in MATLAB, Mathworks, Natick, Massachusetts). A greater filter width was chosen for filtering at the cardiac frequency to accommodate possible changes in heart rate over time. The instantaneous

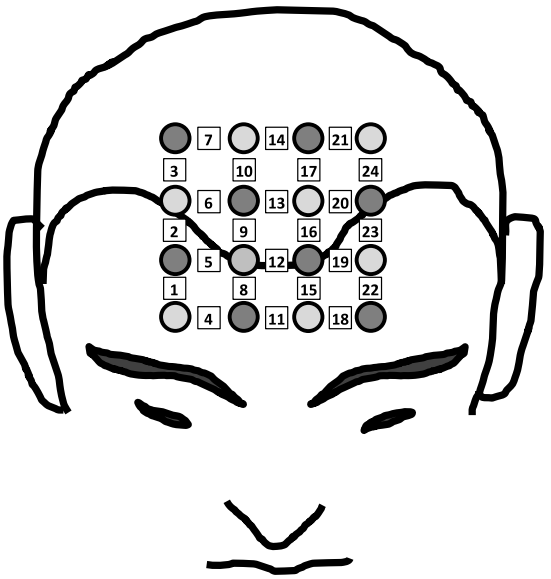

Fig. 3 Optical helmet configuration. Light gray circles correspond to the illumination fibers, dark gray circles correspond to the detection fibers. The squares indicate the measurement channels, numbered from 1 to 24, which correspond to the tissue regions between each source–detector pair used for NIRS measurements.

amplitudes and phases of these signals have been obtained by applying the Hilbert transform to generate the complex analytic signal. Average phase differences, $\mathrm{Arg}(\mathbf{D}) - \mathrm{Arg}(\mathbf{O})$ and $\mathrm{Arg}(\mathbf{i}_{700}) - \mathrm{Arg}(\mathbf{i}_{830})$, where boldface indicates the phasor representation of the band-pass filtered $\Delta O(t)$, $\Delta D(t)$, $i_{700} = \Delta I_{700}(t)/I_{0\_700}$, and $i_{830} = \Delta I_{830}(t)/I_{0\_830}$, and standard deviations were computed by means of circular statistics. In order to avoid any noise or instability introduced by the filter, the first and last 60 s of the filtered signals have been removed before computing averages and standard deviations. To guarantee measurements of regular hemodynamic oscillations in tissue rather than incoherent physiological fluctuations or motion-related artifacts, we further applied the following selection criteria to the data:

i. We only considered those signals where $|\mathbf{D}| > 0.015$ μM and $|\mathbf{O}| > 0.015$ μM, which are amplitude threshold values reported previously to discard frequency components of instrumental noise.[18]
ii. We retained only those signals with a stable phase difference, namely $\sigma_{\mathrm{Arg}(\mathbf{D})-\mathrm{Arg}(\mathbf{O})} < 25$ deg, with σ denoting the circular standard deviation, to measure coherent hemodynamic oscillations.
iii. We discarded those channels that featured signals dominated by motion artifacts (synchronous with the heartbeat, respiration, or other physiological rhythms) or featuring a poor optical contact between the fiber optics and the scalp.

3 Results

3.1 *Cerebral Arterial Saturation from Hemodynamic Oscillations at the Cardiac Frequency*

Out of the 10 subjects measured, four subjects met the criteria of having at least 20 channels with a signal-to-noise ratio

(SNR) > 5 at the cardiac frequency, as determined by the FFT of $\Delta I(t)/I_0$, as described in Sec. 2.8. Of those four subjects, three performed paced breathing at 0.1 Hz (subject nos. 1, 2, and 4). A representative case of filtered $\Delta I_{700}(t)/I_{0\_700}$ and $\Delta I_{830}(t)/I_{0\_830}$ at the cardiac frequency can be seen in Fig. 4(a) for subject no. 1, channel 18. We introduce a phasor notation for the optical intensity (**i**) that follows the same conventions used for the **cbv** and **cbf** phasors. The lower case intensity phasor, **i**, indicates the sinusoidal intensity oscillations relative to the mean value: $\Delta I(t)/I_0$. An average phase difference of $\text{Arg}(\mathbf{i}_{700}) - \text{Arg}(\mathbf{i}_{830}) = 10$ deg was found for this case (subject no. 1, channel 18). After converting the relative intensity changes into $\Delta O(t)$, $\Delta D(t)$, and $\Delta T(t)$ by using the modified Beer–Lambert law and a DPF ratio of 1 (i.e., the same DPF = 6.51 at 700 and 830 nm), we found a phase difference $\text{Arg}(\mathbf{D}) - \text{Arg}(\mathbf{O}) = -269$ deg, as seen in Fig. 4(b). Figures 4(c) and 4(d) show the average phase differences of the intensities at the two wavelengths and of the deoxy- and oxyhemoglobin concentrations, respectively, for all the channels. Error bars show the standard deviation over 10 min of instantaneous phase difference measurements. The black circle in Fig. 4(c) marks the channels with a phase difference that is significantly different from zero.

Since oxy- and deoxyhemoglobin oscillations, as shown in Fig. 4(b), are not in phase with each other, $(|\mathbf{O}|/|\mathbf{T}|) \neq [|\mathbf{O}|/(|\mathbf{O}| + |\mathbf{D}|)]$. Therefore, calculating $S^{(a)}$ as $|\mathbf{O}|/|\mathbf{T}|$ or $|\mathbf{O}|/(|\mathbf{O}| + |\mathbf{D}|)$ yields two different results. Such a difference is seen in Fig. 5 for subject no. 1 and for all measurement channels. The ratio $|\mathbf{O}|/|\mathbf{T}|$ is shown by the black circles and often takes values of $S^{(a)} > 1$, which is of course unreasonable. The ratio $|\mathbf{O}|/(|\mathbf{O}| + |\mathbf{D}|)$ is shown by the gray squares and yields values of $S^{(a)} < 0.98$.

Figure 6 shows the results for channel 18 of subject no. 1 as a phasor diagram. The average phase difference for $\text{Arg}[\mathbf{D}] - \text{Arg}[\mathbf{O}] = 91$ deg (or −269 deg). Based on Eqs. (20)–(27) and the assumption $S^{(a)} = 0.98$, we calculated $\mathbf{O}_F$ and $\mathbf{D}_F$, as well as $\mathbf{O}_V$ and $\mathbf{D}_V$. $\text{Arg}[\mathbf{O}_F] - \text{Arg}[\mathbf{O}]$ was found to be −67 deg. The phasor diagram clearly shows that the flow component of oxyhemoglobin oscillations is much smaller than the volume component ($|\mathbf{O}_F| \ll |\mathbf{O}_V|$), while the magnitudes of $\mathbf{D}_F$ and $\mathbf{D}_V$ are comparable. For this particular case, $|\mathbf{O}|/|\mathbf{T}|$ yields 1.0, which overestimates the set value of arterial saturation (0.98), while $|\mathbf{O}|/(|\mathbf{O}| + |\mathbf{D}|)$ yields 0.95, which underestimates it.

While the fact that $\text{Arg}[\mathbf{D}] - \text{Arg}[\mathbf{O}] \neq 0$ is already indicative of CBF influences on the measured hemoglobin concentration oscillations, the specific value of this phase difference also depends on the ratio of the DPFs at the two wavelengths, $\text{DPF}_{700}/\text{DPF}_{830}$. Since the measurements were performed with a CW domain system, we did not measure the DPFs. We have therefore evaluated the effect of the DPF ratio on $\text{Arg}[\mathbf{D}] - \text{Arg}[\mathbf{O}]$ as well as $\text{Arg}[\mathbf{O}_F] - \text{Arg}[\mathbf{O}]$ (data not shown). We found that the DPF ratio would need to extend outside literature values (0.9 to 1.1)[38] in order to result in $\text{Arg}[\mathbf{D}] - \text{Arg}[\mathbf{O}] = 0$ for all channels. Hence, the DPF ratio cannot account for the phase difference between **D** and **O** measured in most channels, but CBF effects do, as we show next.

We have used our hemodynamic model, specifically Eqs. (34) and (35), to estimate $\text{Arg}[\mathbf{D}] - \text{Arg}[\mathbf{O}]$ and $\text{Arg}[\mathbf{O}_F] - \text{Arg}[\mathbf{O}]$. As described in Eqs. (34) and (35), we have assumed the venous volume oscillation to be negligible. Furthermore, we have set the frequency of oscillations to $\omega/(2\pi) = 1$ Hz to represent a typical cardiac frequency. At a frequency of 1 Hz, which is significantly higher than the cutoff frequency of the RC high-pass filter used to model cerebral autoregulation, the transfer function in Eq. (4) becomes a factor of about 1, thus simplifying Eq. (28) to

$$\mathbf{cbf}(\omega_{\text{hr}} \sim 1\ \text{Hz}) = k\,\mathbf{cbv}(\omega_{\text{hr}} \sim 1\ \text{Hz}) = k\frac{\mathbf{T}(\omega_{\text{hr}})}{T_0}. \qquad (38)$$

We calculated the phase differences $\text{Arg}[\mathbf{D}] - \text{Arg}[\mathbf{O}]$ and $\text{Arg}[\mathbf{O}_F] - \text{Arg}[\mathbf{O}]$ for a physiological range of values of the model parameters. It shall be pointed out that these phase differences are independent of the value of T_0, the cerebral hemoglobin concentration, which has a typical value of 57.5 μM.[39,40] Specifically, the model parameters were iterated within their physiological ranges and histograms of phase differences were obtained. The model parameters, and their considered physiological ranges,[13,16] were capillary blood transit time $t^{(c)} = 0.4$ to 2 s, venous blood transit time $t^{(v)} = 2$ to 7 s, inverse of the modified Grubb's exponent $k = 2$ to 5, rate constant of oxygen diffusion $\alpha = 0.2$ to 1.4 s^{-1}, and arterial saturation $S^{(a)} = 0.94$ to 1.

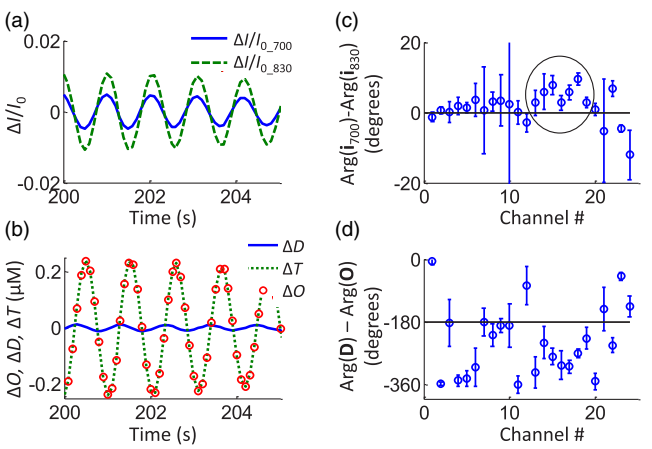

Fig. 4 Representative dataset for subject no. 1 at the cardiac frequency. (a) Band-pass filtered time traces of $\Delta I/I_0$ at both wavelengths for channel 18. (b) The corresponding time traces of ΔO, ΔD, and ΔT with $\text{Arg}(\mathbf{D}) - \text{Arg}(\mathbf{O}) = -269$ deg. Average phase differences between (c) the intensities at two wavelengths, and (d) the deoxy- and oxyhemoglobin concentrations. The circle in panel (c) encloses those channels where the phase differences are significantly different from zero.

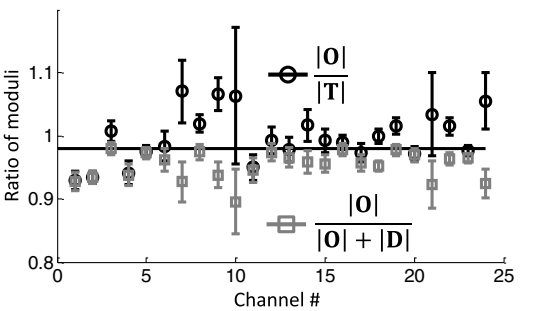

Fig. 5 Ratio of the amplitudes of measured hemoglobin concentration oscillations at the cardiac frequency for subject no. 1 for all channels. Since **O** and **D** are not in phase, it follows that $|\mathbf{O}|/|\mathbf{T}|$ (black circles) does not equal $|\mathbf{O}|/(|\mathbf{O}| + |\mathbf{D}|)$ (gray squares).

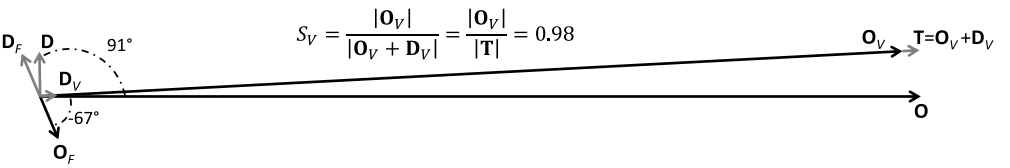

Fig. 6 Representative phasor diagram for subject no. 1, channel 18, at the cardiac frequency. Based on assuming $S^{(a)} = 0.98$, $\mathbf{O}_F$ and $\mathbf{D}_F$, as well as $\mathbf{O}_V$ and $\mathbf{D}_V$ could be calculated as shown.

The histograms in Fig. 7 show the computed phase differences using the model equations. $\text{Arg}[\mathbf{D}] - \text{Arg}[\mathbf{O}]$ ranges from −342 to −215 deg [Fig. 7(a) light gray], with a peak at −255 deg. $\text{Arg}[\mathbf{O}_F] - \text{Arg}[\mathbf{O}]$ shows a much smaller spread of values, ranging from −91 to −34 deg [Fig. 7(b) light gray], with a peak at −72 deg. The dark gray histograms show the experimental data. In order to obtain the histogram of experimental $\text{Arg}[\mathbf{O}_F] - \text{Arg}[\mathbf{O}]$, $S^{(a)}$ was assumed to be 0.98. The model prediction for $\text{Arg}[\mathbf{D}] - \text{Arg}[\mathbf{O}]$ and $\text{Arg}[\mathbf{O}_F] - \text{Arg}[\mathbf{O}]$ fall right into the range of the measured values. The wider spread in the experimental data may be attributed to errors in the phase measurements, especially in channels with lower SNR, and to the set DPF ratio, which may vary across the measurement channels.

Instead of setting $S^{(a)} = 0.98$ in order to obtain $\text{Arg}[\mathbf{O}_F] - \text{Arg}[\mathbf{O}]$, we also calculated $S^{(a)}$ by setting $\text{Arg}[\mathbf{O}_F] - \text{Arg}[\mathbf{O}]$ based on the model prediction, as described in Sec. 2.4. For this, we set $\text{Arg}[\mathbf{O}_F] - \text{Arg}[\mathbf{O}] = -72$ deg, which is the average phase difference found by using the model. Using this phase difference, the average arterial saturation over all subjects and channels was found to be $S^{(a)} = 0.96 \pm 0.02$. In comparison, without taking into account blood flow contributions, we found $(|\mathbf{O}|/|\mathbf{T}|) = 0.97 \pm 0.02$ and $[|\mathbf{O}|/(|\mathbf{O}| + |\mathbf{D}|)] = 0.93 \pm 0.09$. We also considered the spread of the model predictions for $\text{Arg}[\mathbf{O}_F] - \text{Arg}[\mathbf{O}]$, namely $\text{Arg}[\mathbf{O}_F] - \text{Arg}[\mathbf{O}] = -72 \pm 11$ deg, resulting in the range from −83 to −61 deg (mean ± standard deviation). Correspondingly, we found $S^{(a)} = 0.96 \pm 0.02$, for $\text{Arg}[\mathbf{O}_F] - \text{Arg}[\mathbf{O}] = -83$ deg and $S^{(a)} = 0.96 \pm 0.02$, for $\text{Arg}[\mathbf{O}_F] - \text{Arg}[\mathbf{O}] = -61$ deg, with errors given by the standard deviation over all channels and subjects. Therefore, the exact value of $\text{Arg}[\mathbf{O}_F] - \text{Arg}[\mathbf{O}]$ does not play a crucial role in the determination of the value of $S^{(a)}$.

3.2 *Cerebral Oxygen Saturation of Hemoglobin of the Vascular Compartment Oscillating at the Respiration Frequency*

Figure 8 shows a representative dataset for subject no. 1 during paced breathing at a frequency of 0.1 Hz. The filtered time traces of $\Delta I_{700}(t)/I_{0\_700}$ and $\Delta I_{830}(t)/I_{0\_830}$, as well as $\Delta O(t)$, $\Delta D(t)$, and $\Delta T(t)$ at the respiration frequency of 0.1 Hz are shown. An average phase difference of $\text{Arg}(\mathbf{i}_{700}) - \text{Arg}(\mathbf{i}_{830}) = 99 \pm 17$ deg was found for channel 18. The phase difference $\text{Arg}[\mathbf{D}] - \text{Arg}[\mathbf{O}]$ was found to be 200 ± 10 deg. Figures 8(c) and 8(d) show the phase difference of the intensity phasors and of $\mathbf{D}$ and $\mathbf{O}$, respectively, for all channels of subject no. 1.

As described above (Sec. 3.1) in the case of data filtered at the cardiac frequency, the model was used to predict $\text{Arg}[\mathbf{D}] - \text{Arg}[\mathbf{O}]$ and $\text{Arg}[\mathbf{O}_F] - \text{Arg}[\mathbf{O}]$ for the data filtered at the respiration frequency of 0.1 Hz (as applied for 1 Hz as well). The model parameters were iterated as described above, but setting $S^{(a)} = 98\%$. While the autoregulation high-pass filter did not influence the phase of the hemoglobin concentration oscillations at 1 Hz (which is much higher than the filter cutoff frequency), it does at 0.1 Hz (which is much closer to the filter cutoff frequency). The cutoff frequency of autoregulation has been set to $f_c^{(\text{AR})} = 0.03$ Hz, which is a typical value we found previously.[17] While venous volume oscillations could be neglected at the cardiac frequency, both arterial and venous volume oscillations have been taken into account for the paced breathing protocol at 0.1 Hz. The reason for taking arterial volume changes into account is that it is known that mean arterial blood pressure (MAP), which is directly linked to arterial blood volume changes, is oscillating with paced breathing.[19] Specifically, histograms of the phase differences $\text{Arg}[\mathbf{D}] - \text{Arg}[\mathbf{O}]$ and $\text{Arg}[\mathbf{O}_F] - \text{Arg}[\mathbf{O}]$ were generated for three scenarios: (a) $\mathbf{T} = \mathbf{T}^{(a)}$, i.e., assuming no venous volume oscillations; (b) $\mathbf{T} = \mathbf{T}^{(a)} + \mathbf{T}^{(v)}$, i.e., assuming both arterial and venous contributions to hemoglobin concentration oscillations; (c) $\mathbf{T} = \mathbf{T}^{(v)}$, i.e., assuming no arterial volume oscillations. It shall be pointed out that these three scenarios refer to the amplitudes of the

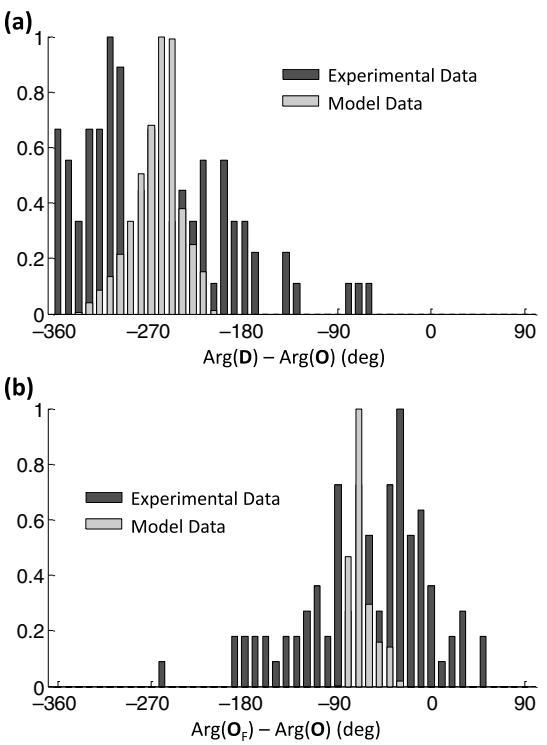

Fig. 7 Model prediction and experimental $\text{Arg}[\mathbf{D}] - \text{Arg}[\mathbf{O}]$ and $\text{Arg}[\mathbf{O}_F] - \text{Arg}[\mathbf{O}]$, at the cardiac frequency. The model predictions for the phase differences are shown by the histograms in light gray and the experimental results in dark gray. Experimental data are shown for all four subjects and all channels per subject. (a) $\text{Arg}[\mathbf{D}] - \text{Arg}[\mathbf{O}]$ and (b) $\text{Arg}[\mathbf{O}_F] - \text{Arg}[\mathbf{O}]$. In order to obtain the experimental $\text{Arg}[\mathbf{O}_F] - \text{Arg}[\mathbf{O}]$, $S^{(a)} = 0.98$ was assumed. Histograms were normalized to better show the phase differences between experimental data and model prediction.

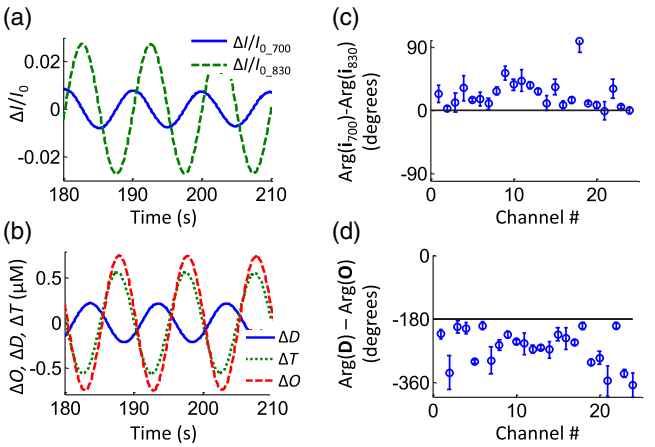

Fig. 8 Representative dataset for subject no. 1 during paced breathing at 0.1 Hz. (a) Band-pass filtered time traces of $\Delta I/I_0$ at both wavelengths for channel 18. (b) The corresponding time traces of ΔO, ΔD, and ΔT. Average phase differences between (c) the intensities at two wavelengths, and (d) the deoxy- and oxyhemoglobin concentrations.

oscillations (changes) of the arterial and venous blood volumes, not to the relative contributions of arterial blood versus venous blood. For the case of $\mathbf{T} = \mathbf{T}^{(a)} + \mathbf{T}^{(v)}$, we have assumed that $\rho^{(v)} = 1/2$; hence, $\mathbf{T}^{(a)} = \mathbf{T}^{(v)}$. In order to achieve $\mathbf{T}^{(a)} = \mathbf{T}^{(v)}$ with the hemodynamic model, we set to the same value the steady state blood volumes of the two vascular compartments, specifically $\mathrm{CBV}_0^{(a)}/\mathrm{CBV}_0 = \mathrm{CBV}_0^{(v)}/\mathrm{CBV}_0 = 0.2$ based on literature,[41] and the oscillatory changes in the blood volumes; hence, $\mathbf{cbv}^{(a)} = \mathbf{cbv}^{(v)}$. The corresponding histograms are seen in Fig. 9, with the three colors corresponding to the three different scenarios (a), (b), and (c) defined above.

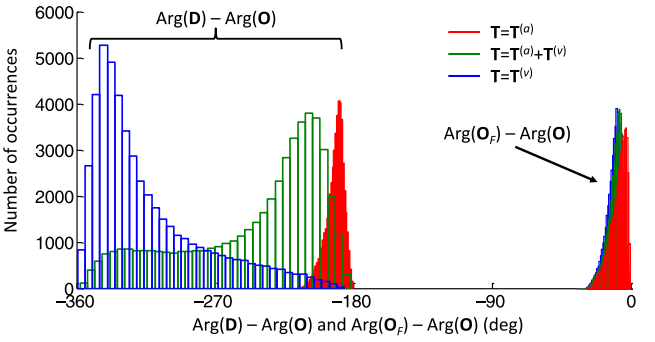

Fig. 9 Histograms of model predictions for $\mathrm{Arg}[\mathbf{D}] - \mathrm{Arg}[\mathbf{O}]$ and $\mathrm{Arg}[\mathbf{O}_F] - \mathrm{Arg}[\mathbf{O}]$ at the paced breathing frequency of 0.1 Hz. Three different scenarios were simulated, with $\mathbf{T} = \mathbf{T}^{(a)}$ (red), $\mathbf{T} = \mathbf{T}^{(a)} + \mathbf{T}^{(v)}$, with $\mathbf{T}^{(a)} = \mathbf{T}^{(v)}$ (green), and $\mathbf{T} = \mathbf{T}^{(v)}$ (blue). While $\mathrm{Arg}[\mathbf{D}] - \mathrm{Arg}[\mathbf{O}]$ varies over a wide range of possible values, $\mathrm{Arg}[\mathbf{O}_F] - \mathrm{Arg}[\mathbf{O}]$ peaks in a small range of values between −9 and −4 deg.

While $\mathrm{Arg}[\mathbf{D}] - \mathrm{Arg}[\mathbf{O}]$ varies considerably over the different scenarios considered (Fig. 9, left), $\mathrm{Arg}[\mathbf{O}_F] - \mathrm{Arg}[\mathbf{O}]$ is strongly peaked between −9 and −4 deg, regardless of which compartment is the source of volume changes and parameters of the model (Fig. 9, right).

We have assumed a value of −7 deg for $\mathrm{Arg}[\mathbf{O}_F] - \mathrm{Arg}[\mathbf{O}]$, which is within the narrow range −9 to −4 deg predicted by the model. Using this value, we have found S_V from Eq. (29) and phasors $\mathbf{O}_V$, $\mathbf{O}_F$, $\mathbf{D}_V$, and $\mathbf{D}_F$ from Eqs. (20)–(27). Figure 10 shows the solution as a phasor diagram for the case of subject no. 1, channel 18, where one can see the flow and volume contributions to the hemoglobin concentration phasors. The oxygen saturation of hemoglobin of the volume-oscillating vascular compartment was found to be $S_V = 0.67$. The measured angle between $\mathbf{D}$ and $\mathbf{O}$ was $\mathrm{Arg}[\mathbf{D}] - \mathrm{Arg}[\mathbf{O}] = 160$ deg (or −200 deg). Based on the model predictions reported in Fig. 9, this phase difference between $\mathbf{D}$ and $\mathbf{O}$ is close to the peak value for the case $\mathbf{T} = \mathbf{T}^{(a)} + \mathbf{T}^{(v)}$ (green histogram) and falls on the tails of the distributions for $\mathbf{T} = \mathbf{T}^{(a)}$ and $\mathbf{T} = \mathbf{T}^{(v)}$. This result suggests that both arterial and venous blood may contribute to the volume oscillating compartment, in agreement with the observation that MAP oscillates at the respiration frequency,[19] which may induce arterial volume oscillations in the brain.

Using all 24 channels from the three subjects investigated with the paced breathing protocol, we calculated $|\mathbf{O}|/|\mathbf{T}|$ and $|\mathbf{O}|/(|\mathbf{O}| + |\mathbf{D}|)$. The results are reported in the histograms of Fig. 11. The average of $|\mathbf{O}|/|\mathbf{T}|$ is 1.1 ± 0.14, and the average of $|\mathbf{O}|/(|\mathbf{O}| + |\mathbf{D}|)$ is 0.88 ± 0.05. As discussed above in Sec. 2.4 [see Eq. (37)], out-of-phase oscillations of oxy- and deoxyhemoglobin concentrations results in $|\mathbf{O} + \mathbf{D}| \neq |\mathbf{O}| + |\mathbf{D}|$, and hence the difference between these ratios.

By assuming the value of −7 deg for $\mathrm{Arg}[\mathbf{O}_F] - \mathrm{Arg}[\mathbf{O}]$ on the basis of model predictions, we calculated the oxygen saturation of hemoglobin of the volume-oscillating vascular compartment, S_V for all subjects and channels. The resulting histogram of $S_V = |\mathbf{O}_V|/|\mathbf{T}|$ is reported in Fig. 11 and features a mean and standard deviation of $\langle S_V \rangle = 0.66 \pm 0.14$. Knowledge or an estimation of the factor $\rho^{(v)}$ and the arterial saturation $S^{(a)}$ allows for the determination of the venous saturation $S^{(v)}$ from the volume-oscillating compartment oxygen saturation of hemoglobin S_V. For example, assuming $\rho^{(v)} = 1/2$, hence $\mathbf{T}^{(a)} = \mathbf{T}^{(v)}$, and $S^{(a)} = 0.98$, the measured value $S_V = 0.66 \pm 0.14$ translates into a venous saturation $S^{(v)} = 0.35 \pm 0.28$ [on the basis of Eq. (16)]. Of course, a greater value of $\rho^{(v)}$ would yield a higher venous saturation. The average phase difference for all channels and subject was found to be $\mathrm{Arg}[\mathbf{O}_F] - \mathrm{Arg}[\mathbf{O}] = -221 \pm 16$ deg. This phase difference falls within the green curve in Fig. 9, where $\mathbf{T}^{(a)} = \mathbf{T}^{(v)}$. However, in general, it is not expected that the relative proportion of arterial and venous volume is constant across all channels and subjects, so that the assumption of $\rho^{(v)}$ and its constant value

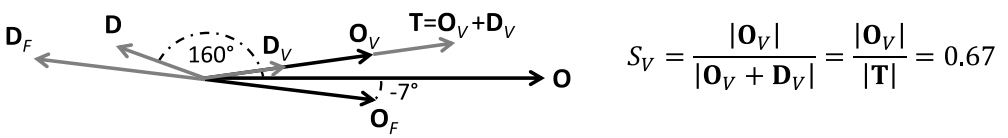

Fig. 10 Phasor diagram for subject no. 1, channel 18, at the paced breathing frequency of 0.1 Hz, obtained by assuming $\mathrm{Arg}[\mathbf{O}_F] - \mathrm{Arg}[\mathbf{O}] = -7$ deg, as estimated by the hemodynamic model. The resulting oxygen saturation of hemoglobin of the volume oscillating compartment is $S_V = 0.67$.

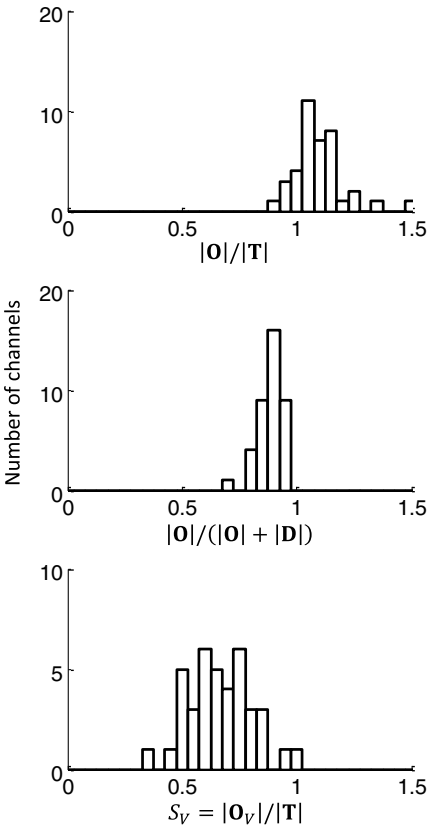

Fig. 11 Results of the analysis of the data during paced breathing for all subjects and measurement channels, demonstrating the difference between the ratios of $|\mathbf{O}|/|\mathbf{T}|$, $|\mathbf{O}|/(|\mathbf{O}|+|\mathbf{D}|)$, and reporting the measured oxygen saturation of hemoglobin of the volume-oscillating vascular compartment. The mean values of the measured quantities were $|\mathbf{O}|/|\mathbf{T}| = 1.1 \pm 0.14$, $|\mathbf{O}|/(|\mathbf{O}|+|\mathbf{D}|) = 0.88 \pm 0.05$, and $\langle S_V \rangle = 0.66 \pm 0.14$.

across all subjects and measurement channels is affected by some level of uncertainty, which affects the mean value and variance of $S^{(v)}$.

4 Discussion

4.1 *Oxygen Saturation of Hemoglobin of Volume-Oscillating Vascular Compartments*

Pulse oximetry and spiroximetry are both based on the assumption that the measured oscillatory changes are based on volume changes alone. In case of pulse oximetry, the arterial compartment is dominant, whereas spiroximetry relies on the respiratory signals being dominated by the venous compartment. Both methods are then based on taking the ratio between the magnitudes of oxyhemoglobin oscillations to total hemoglobin oscillations to obtain a measure of the volume oscillating oxygen saturation of hemoglobin.[4,22,26] It shall be pointed out that in pulse oximetry technically, the ratio of intensity changes is typically used, which however can be translated into changes in oxy- and deoxyhemoglobin.[4] Both methods are only valid if the underlying source of signal changes is based on blood volume changes and if blood flow contributions can be neglected. While this may be the case in tissue other than the brain,[1,4,14,22] neglecting blood flow changes in the brain is questionable. Indeed, studies applying spiroximetry to measure cerebral venous saturation have commented on the fact that measured hemodynamic oscillations are out of phase,[23,25,26] attributing this fact to blood flow changes and invalidating the assumption of spiroximetry. We have shown here that the idea of exploiting blood volume oscillations for measuring $S^{(a)}$ and $S^{(v)}$ by simply taking a ratio of the magnitudes of $\Delta O/\Delta T$, ($|\mathbf{O}|/|\mathbf{T}|$), is not strictly correct and can be at best only an approximation when measuring oscillations of cerebral concentrations of oxy- and deoxyhemoglobin. Even at the cardiac frequency, where arterial volume changes are indeed the dominant source of optical signal changes, CBF oscillations may provide some contributions as well. This is best seen in Figs. 4 and 8, where we have shown that oxy- and deoxyhemoglobin concentrations oscillate out of phase with each other. This phase difference cannot be explained by wrong assumptions in the DPF ratio at the two wavelengths. Of course, the issue is to identify those cases where neglecting the blood flow contributions to the measured optical signals is acceptable and those where it is not: in this article, we have presented a quantitative tool to address this issue.

In the case of hemodynamic oscillations at the cardiac frequency, we have assumed $S^{(a)} = 0.98$ in order to calculate $\mathbf{O}_V$ and $\mathbf{O}_F$ using Eqs. (20)–(27). However, our hemodynamic model could also be used to first estimate $\mathrm{Arg}[\mathbf{O}_F] - \mathrm{Arg}[\mathbf{O}]$ (a phase difference that we have found to be peaked at -72 deg in Fig. 7 for 1 Hz oscillations) and then determine $S^{(a)}$ using Eqs. (20)–(27) or Eqs. (27)–(31). By setting a value of -72 deg for $\mathrm{Arg}[\mathbf{O}_F] - \mathrm{Arg}[\mathbf{O}]$, we have found $S^{(a)} = 0.96 \pm 0.02$. This latter procedure is even more relevant in the case of hemodynamic oscillations at the respiration frequency, as observed in the paced breathing protocol reported here. In this case, the lower paced-breathing frequency of 0.1 Hz (versus ~1 Hz for the cardiac frequency) results in blood flow oscillations that lead blood volume oscillations, as described by the high-pass relationship of Eq. (28), and a smaller phase lag of $\mathbf{O}_F$ versus $\mathbf{O}$. Such a phase difference, $\mathrm{Arg}[\mathbf{O}_F] - \mathrm{Arg}[\mathbf{O}]$, depends on the assumed cutoff frequency of autoregulation. In this work, we have set the autoregulation cutoff frequency, $f_c^{(\mathrm{AR})}$, at 0.03 Hz, and found that $\mathrm{Arg}[\mathbf{O}_F] - \mathrm{Arg}[\mathbf{O}]$ is centered at -7 deg (see Fig. 9) for 0.1 Hz oscillations. While this cutoff frequency is a good approximation based on previous results,[17,18] the exact value was unknown here. Varying $f_c^{(\mathrm{AR})}$ from 0.01 to 0.05 Hz, we have found peak values of $\mathrm{Arg}[\mathbf{O}_F] - \mathrm{Arg}[\mathbf{O}]$ at -13 deg for $f_c^{(\mathrm{AR})} = 0.01$ Hz and -1 deg for $f_c^{(\mathrm{AR})} = 0.05$ Hz. On the basis of these results, considering also that the width of the distribution of $\mathrm{Arg}[\mathbf{O}_F] - \mathrm{Arg}[\mathbf{O}]$ does not increase by more than 5 deg over the autoregulation cutoff frequencies considered, we do not expect the uncertainty in $f_c^{(\mathrm{AR})}$ to significantly impact the results for S_V.

4.2 *Venous Saturation Measurements*

At the respiratory frequency, the common assumption made in literature is that the signal is dominated by venous volume changes.[22–26] Based on spiroximetry, as well as low frequency oscillation ratios, Leung et al.[23] found values of venous saturation between 0.55 and 0.71. Lynch et al.,[24] using ventilated pulmonary hypertension pediatric patients, reported a comparison to superior vena cava (SVC) saturation. The found values were in good agreement (59.6 for spiroximetry versus 0.64 for SVC). However, using healthy adults and regular respiration, the average value found was 0.79 ± 0.07, which is in good agreement

with our value of $\langle|\mathbf{O}|/(|\mathbf{O}|+|\mathbf{D}|)\rangle = 0.88 \pm 0.05$. Both these values are higher than jugular venous saturation, which is typically reported to be between 0.55 and 0.75.[42] Wolf et al.[26] also reported cerebral venous saturation based on spiroximetry, with reported values of 0.73 ± 0.09, also greater than expected values. The same group did also mention an out of phase behavior between oxy- and deoxyhemoglobin oscillations, acknowledging the fact that blood flow changes may influence the results. Based on these reported values and results presented here, $|\mathbf{O}|/(|\mathbf{O}|+|\mathbf{D}|)$ will overestimate the oxygen saturation of hemoglobin, due to uncorrected blood flow influences. The results presented here are demonstrating that it is possible to correct for such influences by disentangling $\mathbf{O}_V$ and $\mathbf{O}_F$. With this, we have found the volume oscillating compartment oxygen saturation of hemoglobin to be $\langle S_V\rangle = 0.66 \pm 0.14$, which falls within the typically measured oxygen saturation of hemoglobin in the jugular vein,[42] indicating that the respiratory signals are indeed dominated by venous blood.

However, an arterial influence on the respiratory signals may also be possible. Once the oxygen saturation of hemoglobin of a volume-oscillating vascular compartment is determined, one is left with its interpretation on the basis of the arterial, capillary, and venous composition of the oscillatory blood volume. In this work, we emphasized on brain measurements and hence we neglected contributions to blood volume oscillations from the capillary bed.[30–35] The question to tackle then pertains to the arterial and venous contributions to blood volume oscillations.

We have evaluated three different scenarios of possible blood volume oscillations, specifically $\mathbf{T} = \mathbf{T}^{(a)}$, $\mathbf{T} = \mathbf{T}^{(a)} + \mathbf{T}^{(v)}$, and $\mathbf{T} = \mathbf{T}^{(v)}$. For $\mathbf{T} = \mathbf{T}^{(a)} + \mathbf{T}^{(v)}$, the underlying assumption was that arterial volume changes and venous volume changes occur synchronously (so that the phasors $\mathbf{T}^{(a)}$ and $\mathbf{T}^{(v)}$ are in phase with each other). If, however, arterial and venous volume changes are not in phase with each other, $\mathrm{Arg}[\mathbf{T}^{(a)}] - \mathrm{Arg}[\mathbf{T}^{(v)}] \neq 0$ deg, it follows that $|\mathbf{T}^{(a)}| + |\mathbf{T}^{(v)}| \neq |\mathbf{T}^{(a)} + \mathbf{T}^{(v)}|$, and separating arterial from venous volume oscillations would not be possible in the absence of additional information.

In order to separate the arterial and venous volume contributions to the optical signals, the factor $\rho^{(v)}$ (which represents the ratio of the venous-to-total oscillatory blood volume) must be known. A direct measurement of $\rho^{(v)}$ may not be possible, even though specially designed physiological maneuvers may be used to estimate it. Of course, there may be cases where it can be reasonably assumed that the volume-oscillating vascular compartment is solely arterial ($\rho^{(v)} = 0$) or venous ($\rho^{(v)} = 1$). We stress again, however, that even in these special cases where the source of blood volume oscillations are known, one may still need to account for oscillatory blood flow contributions to the optical signals. This latter point was the main objective of this work.

5 Conclusion

We have presented an analytical method to translate dynamic NIRS measurements of cerebral hemoglobin concentrations [$\Delta O(t)$ and $\Delta D(t)$] into the oxygen saturation of hemoglobin of the volume-oscillating vascular compartment, S_V, without relying on the assumption that blood volume changes are the only source of the dynamics of the measured optical signals. This result requires taking into account the potential contributions of blood flow dynamics, which may indeed yield non-negligible contributions to the optical signals. These considerations are particularly significant in cerebral NIRS measurements. The methods presented can be applied to absolute local measurements of arterial and venous saturation in brain tissue, provided that one can estimate the relative contributions of arterial and venous compartments to the volume-oscillating vascular bed. Achieving accurate measures of cerebral $S^{(a)}$ and $S^{(v)}$ is highly significant for both research and clinical applications, because such measurements provide information on focal cerebral oxygen extraction fraction and metabolic demand.

Acknowledgments

This research is supported by the National Institutes of Health, grant no. R01-CA154774.

References

1. T. Aoyagi and K. Miyasaka, "The theory and applications of pulse spectrophotometry," *Anesth. Analg.* **94**(1 Suppl), S93–S95 (2002).
2. T. Aoyagi and K. Miyasaka, "Pulse oximetry: its invention, contribution to medicine, and future tasks," *Anesth. Analg.* **94**(1 Suppl), S1–S3 (2002).
3. P. D. Mannheimer, "The light-tissue interaction of pulse oximetry," *Anesth. Analg.* **105**(6 Suppl), S10–S107 (2007).
4. M. Nitzan, A. Romem, and R. Koppel, "Pulse oximetry: fundamentals and technology update," *Med. Dev.* **7**, 231–239 (2014).
5. P. A. Kyriacou, "Pulse oximetry in the oesophagus," *Physiol. Meas.* **27**(1), R1–R35 (2006).
6. B. J. Wilson et al., "The accuracy of pulse oximetry in emergency department patients with severe sepsis and septic shock: a retrospective cohort study," *BMC Emerg. Med.* **10**, 9 (2010).
7. J. L. Reuss, "Multilayer modeling of reflectance pulse oximetry," *IEEE Trans. Biomed. Eng.* **52**(2), 153–159 (2005).
8. J. L. Reuss and D. Siker, "The pulse in reflectance pulse oximetry: modeling and experimental studies," *J. Clin. Monit. Comput.* **18**(4), 289–299 (2004).
9. K. H. Shelley et al., "The effect of venous pulsation on the forehead pulse oximeter wave form as a possible source of error in Spo_2 calculation," *Anesth. Analg.* **100**(3), 743–747 (2005).
10. G. S. Agashe, J. Coakley, and P. D. Mannheimer, "Forehead pulse oximetry: Headband use helps alleviate false low readings likely related to venous pulsation artifact," *Anesthesiology* **105**(6), 1111 (2006).
11. G. Dietsche et al., "Fiber-based multispeckle detection for time-resolved diffusing-wave spectroscopy: characterization and application to blood flow detection in deep tissue," *Appl. Opt.* **46**(35), 8506–8514 (2007).
12. J. Seki et al., "Velocity profiles in the rat cerebral microvessels measured by optical coherence tomography," *Clin. Hemorheol. Microcirc.* **34**(1–2), 233–239 (2006).
13. S. Fantini, "Dynamic model for the tissue concentration and oxygen saturation of hemoglobin in relation to blood volume, flow velocity, and oxygen consumption: implications for functional neuroimaging and coherent hemodynamics spectroscopy (CHS)," *Neuroimage* **85**, 202–221 (2014).
14. M. L. Pierro et al., "Validation of a novel hemodynamic model for coherent hemodynamics spectroscopy (CHS) and functional brain studies with fNIRS and fMRI," *Neuroimage* **85**(Pt 1), 222–233 (2014).
15. J. M. Kainerstorfer, A. Sassaroli, and S. Fantini, "Coherent hemodynamics spectroscopy in a single step," *Biomed. Opt. Express* **5**(10), 3403–3416 (2014).
16. J. M. Kainerstorfer et al., "Practical steps for applying a new dynamic model to near-infrared spectroscopy measurements of hemodynamic oscillations and transient changes: implications for cerebrovascular and functional brain studies," *Acad. Radiol.* **21**(2), 185–196 (2014).
17. J. M. Kainerstorfer et al., "Cerebral autoregulation in the microvasculature measured with near-infrared spectroscopy," *J. Cereb. Blood Flow Metab.* **35**(6), 959–966 (2015).
18. M. L. Pierro et al., "Reduced speed of microvascular blood flow in hemodialysis patients versus healthy controls: a coherent hemodynamics spectroscopy study," *J. Biomed. Opt.* **19**(2), 026005 (2014).
19. M. Reinhard et al., "Oscillatory cerebral hemodynamics—the macro vs. microvascular level," *J. Neurol. Sci.* **250**(1–2), 103–109 (2006).

20. M. E. Wagshul, P. K. Eide, and J. R. Madsen, "The pulsating brain: a review of experimental and clinical studies of intracranial pulsatility," *Fluids Barriers CNS* **8**(1), 5 (2011).
21. S. Fantini, "A haemodynamic model for the physiological interpretation of in vivo measurements of the concentration and oxygen saturation of haemoglobin," *Phys. Med. Biol.* **47**(18), N249–N257 (2002).
22. M. A. Franceschini et al., "Near-infrared spiroximetry: noninvasive measurements of venous saturation in piglets and human subjects," *J. Appl. Physiol.* **92**(1), 372–384 (2002).
23. T. S. Leung et al., "Cerebral tissue oxygen saturation calculated using low frequency haemoglobin oscillations measured by near infrared spectroscopy in adult ventilated patients," *Adv. Exp. Med. Biol.* **614**, 235–244 (2008).
24. J. M. Lynch et al., "Noninvasive optical quantification of cerebral venous oxygen saturation in humans," *Acad. Radiol.* **21**(2), 162–167 (2014).
25. J. Menssen et al., "A method to calculate arterial and venous saturation from near infrared spectroscopy (NIRS)," *Adv. Exp. Med. Biol.* **645**, 135–140 (2009).
26. M. Wolf et al., "Continuous noninvasive measurement of cerebral arterial and venous oxygen saturation at the bedside in mechanically ventilated neonates," *Crit. Care Med.* **25**(9), 1579–1582 (1997).
27. L. Skov et al., "Estimation of cerebral venous saturation in newborn infants by near infrared spectroscopy," *Pediatr. Res.* **33**(1), 52–55 (1993).
28. M. Nitzan et al., "Measurement of oxygen saturation in venous blood by dynamic near infrared spectroscopy," *J. Biomed. Opt.* **5**(2), 155–162 (2000).
29. S. Fantini, "A new hemodynamic model shows that temporal perturbations of cerebral blood flow and metabolic rate of oxygen cannot be measured individually using functional near-infrared spectroscopy," *Physiol. Meas.* **35**(1), N1–N9 (2014).
30. J. L. Chen et al., "Slightly altered permeability-surface area products imply some cerebral capillary recruitment during hypercapnia," *Microvasc. Res.* **48**(2), 190–211 (1994).
31. U. Gobel et al., "Lack of capillary recruitment in the brains of awake rats during hypercapnia," *J. Cereb. Blood Flow Metab.* **9**(4), 491–499 (1989).
32. W. Kuschinsky and O. B. Paulson, "Capillary circulation in the brain," *Cerebrovasc. Brain Metab. Rev.* **4**(3), 261–286 (1992).
33. A. Villringer, "The intravascular susceptibility effect and the underlying physiology of fMRI," *Neuroimage* **62**(2), 995–999 (2012).
34. A. Villringer et al., "Capillary perfusion of the rat brain cortex. An in vivo confocal microscopy study," *Circ. Res.* **75**(1), 55–62 (1994).
35. G. Zoccoli et al., "Brain capillary perfusion during sleep," *J. Cereb. Blood Flow Metab.* **16**(6), 1312–1318 (1996).
36. A. P. Blaber et al., "Transfer function analysis of cerebral autoregulation dynamics in autonomic failure patients," *Stroke* **28**(9), 1686–1692 (1997).
37. R. R. Diehl et al., "Phase relationship between cerebral blood flow velocity and blood pressure. A clinical test of autoregulation," *Stroke* **26**(10), 1801–1804 (1995).
38. R. Zhang et al., "Transfer function analysis of dynamic cerebral autoregulation in humans," *Am. J. Physiol.* **274**(1 Pt 2), H233–H241 (1998).
39. B. Hallacoglu et al., "Absolute measurement of cerebral optical coefficients, hemoglobin concentration and oxygen saturation in old and young adults with near-infrared spectroscopy," *J. Biomed. Opt.* **17**(8), 081406 (2012).
40. V. Quaresima et al., "Bilateral prefrontal cortex oxygenation responses to a verbal fluency task: a multichannel time-resolved near-infrared topography study," *J. Biomed. Opt.* **10**(1), 011012 (2005).
41. F. Cassot et al., "A novel three-dimensional computer-assisted method for a quantitative study of microvascular networks of the human cerebral cortex," *Microcirculation* **13**(1), 1–18 (2006).
42. R. M. Schell and D. J. Cole, "Cerebral monitoring: jugular venous oximetry," *Anesth. Analg.* **90**(3), 559–566 (2000).

Jana M. Kainerstorfer is an assistant professor of biomedical engineering at Carnegie Mellon University. Her research includes noninvasive optical imaging of tissue for disease detection and/or treatment monitoring, with a particular emphasis on diffuse optical spectroscopic imaging (with applications to the brain, breast, skin, and muscle). Her research spans from instrument development to novel data analysis tools all the way to clinical applications. Her research is published in more than 20 peer-reviewed scientific articles.

Angelo Sassaroli is research assistant professor of biomedical engineering at Tufts University. His research interests are within the fields of near-infrared spectroscopy and diffuse optical tomography for monitoring cerebral hemodynamics and breast cancer. He is mainly interested in developing analytical/computational methods for photon migration in tissue. He has coauthored more than 60 peer-reviewed scientific publications.

Sergio Fantini is a professor of biomedical engineering at Tufts University. His research interests are in diffuse optical spectroscopy and imaging of biological tissues, with applications to the human brain (functional imaging and assessment of cerebral hemodynamics), breast (cancer detection and monitoring response to therapy), and skeletal muscle (quantitative tissue oximetry). His research resulted in 11 patents and about 200 scientific publications, and he coauthored with Irving Bigio the textbook *Quantitative Biomedical Optics*.